Boundary-Layer Meteorol (2012) 145:5–25
DOI 10.1007/s10546-012-9742-5

ARTICLE

Structure Function Analysis of Two-Scale Scalar Ramps. Part I: Theory and Modelling

T. M. Shapland · A. J. McElrone · R. L. Snyder · K. T. Paw U

Received: 10 May 2011 / Accepted: 31 May 2012 / Published online: 27 June 2012

Abstract Structure functions are used to study the dissipation and inertial range scales of turbulent energy, to parametrize remote turbulence measurements, and to characterize ramp features in the turbulent field. Ramp features are associated with turbulent coherent structures, which dominate energy and mass fluxes in the atmospheric surface layer. The analysis of structure functions to identify ramp characteristics is used in surface renewal methods for estimating fluxes. It is unclear how commonly observed different scales of ramp-like shapes (i.e., smaller ramps and spikes embedded in larger ramps) influence structure function analysis. Here, we examine the impact of two ramp-like scales on structure function analysis using artificially generated data. The range of time lags in structure function analysis was extended to include time lags typically associated with isotropic turbulence to those larger than the ramp durations. The Van Atta procedure (Arch Mech 29:161–171, 1977) has been expanded here to resolve the characteristics of two-scale ramp models. This new method accurately, and in some cases, exactly determines the amplitude and duration of both ramp scales. Spectral analysis was applied to the structure functions for a broad range of time lags to provide qualitative support for the expanded Van Atta procedure results. The theory reported here forms the foundation for novel methods of analyzing turbulent coherent structures.

Keywords Coherent structures · Structure functions · Surface renewal · Temperature ramps

T. M. Shapland
Department of Viticulture & Enology, University of California, Davis, CA 95616, USA

A. J. McElrone
Crops Pathology and Genetics Research Unit, United States Department of Agriculture-Agricultural Research Service, Davis, CA 95616, USA

R. L. Snyder · K. T. Paw U (✉)
Atmospheric Science, University of California, Davis, CA 95616, USA
e-mail: ktpawu@ucdavis.edu

1 Introduction

Structure functions are a ubiquitous tool in the study of turbulence with applications ranging in scale from the turbulent energy cascade to the identification of turbulent coherent structures. Monin and Yaglom (1975) defined the structure function as the squared differencing operator, which they also referred to as the "second-order structure function". Wyngaard (2010) noted that the spectral transfer function of the differencing operator is approximately sinusoidal, so the structure function filters out eddies that are much larger than the structure-function separation distance parameter. This property makes structure functions suitable to the study of isotropic turbulence and the cascade of energy from large to small scales (Wyngaard 2010). Structure functions have been used with Monin–Obukhov similarity theory to estimate the surface sensible heat flux (Wyngaard et al. 1971; Wyngaard 1973), while second-order structure functions have been used to analyze radar, sodar, lidar and scintillometer data, arriving at scalar fluxes and capping inversion characteristics (Wyngaard and Lemone 1980; Lenschow 1986; Stull 1988).

Structure functions have been used with surface renewal theory (Paw U et al. 1995) to yield estimates of scalar fluxes in the surface layer (Snyder et al. 1996, 1997; Spano et al. 1997, 2000; Chen et al. 1997b; Paw U 2001; Paw U et al. 2005). Surface renewal theory assumes ramp-like scalar patterns in turbulence are manifestations of the turbulent coherent structures thought to dominate surface exchange processes (Gao et al. 1989; Paw U et al. 1995). Structure functions provide a method of determining the turbulent ramp characteristics (Paw U et al. 2005) that is not possible using wavelet analysis since the wavelet shapes are different from the turbulent ramp shapes. By analyzing the scalar time series with multiple orders of structure functions, as described in Van Atta (1977) and hereafter referred to as 'VA', one can arrive at the repetition frequency of coherent structures renewing the surface layer, the amplitude of the scalar ramps, and the surface exchange estimate (Snyder et al. 1996, 1997; Paw U 2001; Paw U et al. 2005).

The VA ramp model consists of a single scale of a repeating ramp shape with uniform amplitude and duration throughout the dataset. In contrast, turbulent scalar data exhibit more than one scale of embedded ramp-like shapes and spikes as seen in traces of high-frequency turbulent scalar data (e.g., Fig. 1 in Paw U et al. 1992; Fig. 1 in Collineau and Brunet 1993b). Paw U et al. (1992) noted that many ramp identification procedures are evaluated by subjective visual inspection of the time series (Blackwelder and Kaplan 1976; Antonia et al. 1983; Collineau and Brunet 1993a,b), but this may overlook ramp scales that are not readily identified by the human eye. To address the subjectivity of ramp detection schemes, Collineau and Brunet (1993a,b) established a method for a less subjective analysis of the Mexican Hat wavelet. Their automated method yielded ramp durations that agreed with their subjective visual estimations from the time series; however, ramp-like features can be observed between the detected events (see Fig. 4 in Collineau and Brunet 1993b), and the number of detections increased with a decrease in the wavelet dilation (length scale) parameter (Collineau and Brunet 1993b). A few reports have noted the embedded ramp-like scales (Spano et al. 1997; Chen et al. 1997a), but the importance of these features has not been addressed in any detail. Smaller shear-driven coherent structures embedded within larger thermal structures, which also appear as ramp shapes in the temperature trace, have been observed in remotely sensed data (Thomas et al. 2006).

The estimation of the efficiency of coherent structures in transporting mass and momentum depends on the detection scheme (Antonia et al. 1983; Gao et al. 1989; Collineau and Brunet 1993b). The discrepancy amongst methods possibly results from differences in the interpretation of the various scales of turbulence (Collineau and Brunet 1993b). Consequently, it is

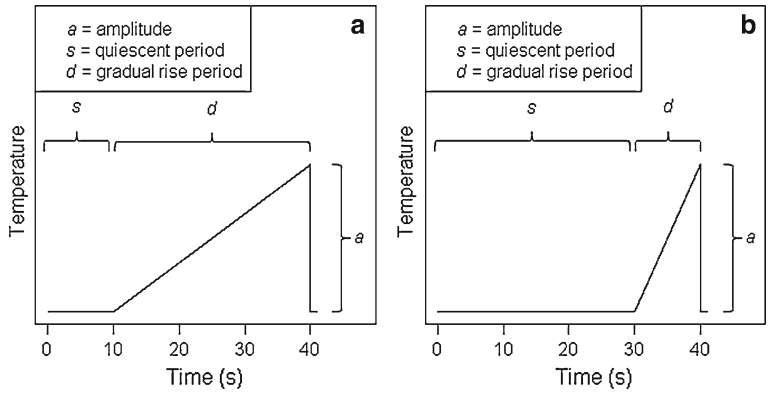

Fig. 1 Model ramp traces for, **a** a persistent ramp, and **b** an intermittent ramp

unclear which turbulent scales are central to the transport process. We propose that smaller scale ramps and ramp-like spikes are the signature of non-flux-bearing, more nearly isotropic, turbulence, and resolving the characteristic amplitude and duration of these shapes will lend insight into small-scale turbulent processes. On the other hand, the characteristics of larger scale ramps provide information on flux-bearing coherent structures and surface renewal.

It is important to evaluate the effect of multiple ramp scales on the VA procedure to resolve ramp characteristics for the following reasons: (1) the procedure does not require a threshold parameter, which decreases subjectivity in ramp detection; (2) it is not clear which ramp scale the VA procedure identifies; and (3) the influence of multiples scales on the VA identified ramp characteristics has not been investigated. A better understanding of the VA procedure using data with multiple ramp scales may elucidate turbulent processes, may improve surface-renewal flux estimates, and may help to objectively resolve the characteristics of more than one ramp scale within the VA procedure framework.

Using artificially generated data, the general effect of two scales (two ramp scales or one ramp scale and one symmetric spike scale) on structure functions and the VA procedure is presented. We report on the application of structure functions over an expanded range of time lags and the use of spectral analysis on the structure functions to detect coherent structure scales. This study provides the theoretical foundation for a new objective method to resolve characteristics of two-scales of turbulent scalar ramp-like shapes (e.g., two ramp scales, or one ramp scale and one symmetric spike scale).

2 Model Description

Throughout, the model time series of identical repeating ramps as proposed by Van Atta (1977) is referred to as the VA ramp model, whereas the method for resolving the ramp amplitude and ramp duration is referred to as the VA procedure. The terms 'VA amplitude' and 'VA ramp period' refer to the values of the ramp amplitude and ramp period as derived using the VA procedure. Together the 'VA amplitude' and the 'VA ramp period' are referred to as the 'VA solutions'.

The VA ramp model is shown in Fig. 1a, b, where the 'ramp amplitude' (a) is the magnitude of the sudden fall (or rise) of the scalar. The interval between the ramp patterns is the 'quiescent period' (s), and the interval when the scalar gradually increases (or decreases) is

Table 1 Model ramp characteristics and derived values using the expanded VA procedure

Model	a_1	d_1	s_1	$\frac{a_1}{(d+s)_1}$	a_2	d_2	s_2	$\frac{a_2}{(d+s)_2}$	d_1 (derived)	$\frac{a_1}{(d+s)_1}$ (derived)	$\frac{a_2}{(d+s)_2}$ (derived)
M1	1.00	50.00	11.00	0.02	–	–	–	–	50.96	0.02	–
M2	1.00	1.40	7.00	0.12	1.00	50.00	11.00	0.02	1.40	0.14	0.02
M3	1.00	7.00	1.40	0.12	1.00	50.00	11.00	0.02	5.31	0.14	0.05
M4	0.50	1.40	7.00	0.06	1.00	50.00	11.00	0.02	2.25	0.05	0.02
M5	1.00	7.00	35.00	0.02	1.00	50.00	11.00	0.02	7.54	0.04	0.02
M6	0.50	2.80	14.00	0.06	1.00	50.00	11.00	0.02	2.24	0.04	0.02

the 'gradual rise period' (d). The sudden fall (or rise) interval of the scalar is the 'microfront'. The 'ramp period' is the sum of the intervals for quiescent period, the gradual rise period, and the microfront. A ramp with the gradual rise period greater than or equal to the quiescent period is referred to as *persistent* (Fig. 1a), even though the quiescent period can occupy up to one half of the ramp period. On the other hand, a ramp series with the gradual rise period less than the quiescent period is referred to as *intermittent* (Fig. 1b).

Temperature ramps similar to those in Fig. 1a are associated with heating of the air by the surface (i.e., a positive sensible heat flux) with the temperature being steady during the quiescent period, rising slowly in the gradual rise period, and falling rapidly (almost instantaneously) in the microfront segment of the trace. Under conditions of negative sensible heat flux, the temperature ramps are inverted with a gradual decrease after the quiescent period, and a rapid temperature rise at the microfront occurrence. The ramp signature in the velocity field can be described in a similar manner to the temperature trace.

The theories developed herein are tested against six prototype ramp models (Table 1), based on phenomena we commonly have observed in turbulent scalar data. The first model (M1) has only one ramp scale and the ramp is persistent; the second (M2) has an intermittent smaller scale ramp, a persistent larger scale ramp, and the amplitudes of both ramp scales are equal, while third model (M3) has persistent smaller and larger ramp scales that have equal amplitudes. The fourth model (M4) is similar to M2, except the amplitudes of the two ramp scales are unequal; the fifth (M5) is also similar to M2, but the ramp periods of the two ramp scales are approximately equal, and the sixth model (M6) has an alternative smaller waveform superimposed onto M1.

The modelling, data processing, analysis, and graphics generation were performed using R software (R Development Core Team 2012).

3 Theory

3.1 Structure Functions of the VA Ramp Model and Review of the VA Procedure

The structure function is defined as the mean value of the time difference of a scalar taken to some power. In discrete terms it is written,

$$\overline{S^n(r)} = \frac{1}{m-j} \sum_{i=1}^{m-j} \left[\left(T_i - T_{i-j} \right)^n \right] \tag{1}$$

where $\overline{S^n(r)}$ is the nth-order structure function, m is the number of points in the time series, j is the sample lag between points, and T_i is the ith element in the scalar time series. The time lag (r) is calculated as the sample lag divided by the sampling frequency $(r = j/f)$.

Van Atta (1977) hypothesized that the scalar time series is the sum of a coherent ramp signal and a random noise signal that was devoid of structure and independent of the coherent signal, allowing his derivation of the following equations:

$$\overline{S^n(r)} = \overline{S^n(r)}_{\text{coherent}} + \overline{S^n(r)}_{\text{random}} = \overline{S^n(r)}_{\text{c}} + \overline{S^n(r)}_{\text{r}}, \tag{2}$$

$$\overline{S^2(r)} = \overline{S^2(r)}_{\text{c}} + \overline{S^2(r)}_{\text{r}}, \tag{3}$$

$$\overline{S^3(r)} = \overline{S^3(r)}_{\text{c}}, \tag{4}$$

$$\overline{S^5(r)} = 10\ \overline{S^2(r)}_{\text{r}}\,\overline{S^3(r)}_{\text{c}} + \overline{S^5(r)}_{\text{c}}. \tag{5}$$

Assuming a model for the joint probability distribution of the ramp amplitude, ramp gradual rise period, and quiescent period, Van Atta (1977) derived the second-order, $(\overline{S^2(r)})$, third-order, $(\overline{S^3(r)})$, and fifth-order, $(\overline{S^5(r)})$, structure functions of the coherent ramp signal as functions of the ramp dimensions and the time lag, given that the time lag parameter (r) is less than the quiescent period (s) and the gradual rise period (d),

$$\overline{S^2(r)_{\text{c}}} = \frac{a^2 r}{(d+s)}\left[1 - \frac{1}{3}\left(\frac{r}{d}\right)^2\right], \tag{6}$$

$$\overline{S^3(r)_{\text{c}}} = \frac{a^3 r}{(d+s)}\left[-1 + \frac{3}{2}\frac{r}{d} - \frac{1}{2}\left(\frac{r}{d}\right)^3\right] \tag{7}$$

$$\overline{S^5(r)_{\text{c}}} = \frac{a^5 r}{(d+s)}\left[-1 + \frac{5}{2}\frac{r}{d} - \frac{10}{3}\left(\frac{r}{d}\right)^2 + \frac{5}{2}\left(\frac{r}{d}\right)^3 - \frac{2}{3}\left(\frac{r}{d}\right)^5\right] \tag{8}$$

where a is the ramp amplitude and $(d+s)$ is the inverse ramp frequency or ramp period. For time lags much shorter than the gradual rise period, Eqs. 6–8 can be simplified into linear expressions.

Combining Eqs. 3–5 with the linear form of Eqs. 6–8, Van Atta (1977) derived solutions for a and $(d+s)$, two ramp characteristics fundamental to surface renewal theory (Paw U et al. 1995; Snyder et al. 1996):

$$0 = a^3 + \left[10\,\overline{S^2(r)} - \frac{\overline{S^5(r)}}{\overline{S^3(r)}}\right] a + 10\,\overline{S^3(r)}, \tag{9}$$

and

$$(d+s) = -\frac{a^3 r}{\overline{S^3(r)}}. \tag{10}$$

Although Van Atta (1977) derived Eqs. 6–8 in probability space, the structure functions herein are derived equivalently using the mean value theorem of integration, which was also used by Chen et al. (1997a).

$$\overline{S^n(r)_{\text{c}}} = \frac{1}{(d+s)}\int_0^{(d+s)} [\Delta T\,(t)]^n\,\mathrm{d}t \tag{11}$$

where $\Delta T\,(t) = T\,(t) - T\,(t-r)$, T is the scalar, and t is time.

3.2 The Dominant Term Approximation: A Convenient Tool in Ramp-Model Derivations

For short time lags, the final term in the structure-function integral, which arises from the drop at the end of the ramp (Appendix 1 and 2), is approximately equal to the entire structure function. We examine the third-order structure function as an example. The final term for the third-order structure-function integral is

$$\int_{(d+s-r)}^{(d+s)} \left[\frac{a}{d}(s-t)\right]^3 \mathrm{d}t = a^3 r\left[-1+\frac{3}{2}\frac{r}{d}-\left(\frac{r}{d}\right)^2+\frac{1}{4}\left(\frac{r}{d}\right)^3\right]. \tag{12}$$

When averaged over the ramp period and simplified into linear form, Eq. 12 is equivalent to the linear form of the entire third-order structure function, Eq. 7.

The dominant term approximation is written as

$$\int_{(d+s-r)}^{(d+s)} [\Delta T\,(t)]^n \,\mathrm{d}t = (-1^n)a^n r \tag{13}$$

and holds true for the second-, third-, and fifth-order structure functions at short time lags.

3.3 Structure Functions of the VA Ramp Model for all Possible Time Lags

The model ramps assumed by Van Atta (1977) repeat throughout the length of the time series, so their structure functions also repeat for time lags longer than the individual ramp scales. The time lags used in Van Atta (1977) were much shorter than the gradual rise period. In contrast, the analytical expressions for all time lags are derived in our study. Wyngaard (2010) described a similar idea in taking the spectral transfer function of the differencing operator. The rationale for examining time lags longer than a ramp period is that the third-order structure function, for example, filters out some types of random noise and its periodicity can yield the coherent structure's ramp period. Thus, spectral analysis of structure functions with respect to the time lag domain, or a related type of frequency analysis, could help identify ramp duration and repetition characteristics.

For each order of structure function (i.e., second, third, and fifth) the derivations yield two sets of discontinuous equations, depending on ramp intermittency. Details of structure-function derivations are presented in the Appendix. Figure 2a, b depicts the second-, third-, and fifth-order structure functions in the time-lag domain for a persistent ramp model and an intermittent ramp model, respectively. The periodic nature of the structure functions is clear (Fig. 2a, b), with both waves loosely resembling sinusoidal functions; however, it is difficult to formally quantify this resemblance and it is beyond the scope of the present study.

3.4 Spectral Decomposition of the Third-Order Structure Function

Following the assumptions of the VA ramp model, the third-order structure function represents the coherent ramp signal without the random noise signal. The periodicity of the ramp signal in the time domain produces a sinusoidal-like periodicity in the third-order structure function in the time-lag domain. If the time series contains more than one ramp scale, then the third-order structure function is approximately the sum of the sinusoidal waves from each ramp scale. Ideally, the discrete Fourier transform (DFT) of the third-order structure function exhibits peaks at frequencies associated with ramp frequencies and coherent structures. The following procedure transforms the ordinates of the DFT into ramp amplitudes.

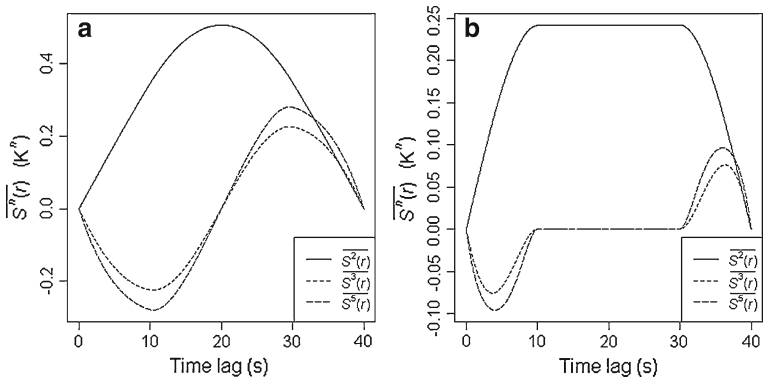

Fig. 2 Second-, third-, and fifth-order structure functions for, **a** a persistent ramp model, and **b** an intermittent ramp model

First, the scaled DFT is obtained from the DFT so that the ordinates correspond to the third-order structure-function waveform amplitudes.

$$(4/n)I\left(f_j\right) = P\left(f_j\right) = \left(A_j^2 + B_j^2\right) \tag{14}$$

where n is the number of points in the time series, f_j are the Fourier frequencies, $I\left(f_j\right)$ is the DFT ordinates, $P\left(f_j\right)$ is the scaled DFT ordinates, A_j^2 are the squared cosine wave amplitudes, and B_j^2 are the squared sine wave amplitudes (Bloomfield 2000). Because the third-order structure function is zero at zero time lag and approximates a sine wave, the cosine amplitude terms (A_j^2) can be dropped, and the square roots of the scaled DFT ordinates, (R_j), correspond to the third-order structure-function waveform amplitudes.

The third-order structure function for short time lags is given by Eq. 7 regardless of intermittency conditions, and the third-order structure function for each ramp frequency approximates a sine wave. Combining Eq. 7 with the scaled DFT, we arrive at the following expression.

$$\overline{S^3(r)_{cj}} = \frac{a_j^3 r}{(d+s)_j}\left[-1 + \frac{3}{2}\frac{r}{d} - \frac{1}{2}\left(\frac{r}{d}\right)^3\right] \cong R_j \sin\frac{2\pi r}{(d+s)_j} \tag{15}$$

where $\overline{S^3(r)_{cj}}$ is the third-order structure function associated with each Fourier frequency, a_j is the ramp amplitude associated with each Fourier frequency, and $(d+s)_j$ is the ramp period associated with each Fourier frequency. For time lags much shorter than the gradual rise period, the higher-order terms in $\overline{S^3(r)_{cj}}$ can be dropped, viz.

$$-\frac{a_j^3 r}{(d+s)_j} \cong R_j \sin\frac{2\pi r}{(d+s)_j}. \tag{16}$$

The sign of the sine wave amplitudes is lost in the DFT, so the sign of the ramp amplitude at each Fourier frequency is also lost. Consequently, the negative sign before the ramp amplitude term in Eq. 14 is dropped, but note that it is recoverable from the sign of the third-order structure function at short time lags—see Eq. 7. Taking the cube root, the ramp amplitude at each of the Fourier frequencies is obtained, hereafter referred to as the ramp spectrum,

$$a_j \cong \left[\frac{(d+s)_j}{r} R_j \sin \frac{2\pi r}{(d+s)_j} \right]^{\frac{1}{3}}. \tag{17}$$

Careful interpretation of the ramp spectrum is necessary because there are numerous sources of departure of the third-order structure function from sinusoidal waveforms. The departure of the third-order structure function from the sine wave form causes leakage in the frequency domain, and its impact is explored in Sect. 4.4.

Ramp-amplitude modulation and ramp-frequency modulation in the time domain cause amplitude and frequency modulation in the third-order structure-function waves, which introduce leakage into the ramp spectrum. Even for ideal ramps, without amplitude or frequency modulations, the third-order structure function of persistent ramps more closely resembles a sine wave than does the third-order structure function of intermittent ramps (Fig. 2a, b). Regression analysis of a sine wave and a third-order structure function can demonstrate that the third-order structure function most closely resembles a sine wave for persistent ramps with values of the quiescent period near one-fourth of the ramp period (not shown). As the quiescent period increases, the third-order structure function becomes less sinusoidal and the spectrum of an intermittent ramp model has its greatest peak at the second harmonic of the ramp frequency.

Leakage is also introduced into the spectrum if the ramp model contains more than a single ramp scale. The third-order structure function is the cubed sum of the terms from each scale. Because the two ramp scales are added together before the structure function is applied, the third-order structure-function wave form is not the sum of the individual third-order structure-function wave forms, which causes departures from sinusoidal forms.

The following common data whitening operations, which are conventional post-processing operations in spectral analysis (Stull 1988; Bloomfield 2000), were performed prior to taking the DFTs. A linear trend removal operation was applied to the time-domain data, because trends cause amplitude modulation in the third-order structure function. The third-order structure function was truncated to half of the number of points in the time-series. As the time lag approaches the duration of the time-series length, the structure-function operation is based on fewer measurement points. In practice, this causes amplitude modulation artefacts in the third-order structure function at time lags approaching the time-series length. Lastly, a cosine bell taper was applied to the initial and final 10 % of the input data to mitigate data window leakage.

3.5 Deriving the Structure Functions and Expanding the VA Procedure for a Two-Scale Ramp Model

The structure function of a ramp model with more than one ramp scale is divided into numerous discontinuous equations, depending on: (1) the number of scales; (2) the relative sizes of the scales; and (3) the intermittency of the scales. This investigation is limited to two-scale ramp models because they provide important insights into structure functions, the VA procedure, coherent-structure characteristics and the surface renewal process for the scope of our study. While it is possible to expand the analysis to ramp models with greater than two scales, such analysis becomes greatly complex and cumbersome, so it is not presented here for the sake of brevity.

Each ramp scale is labelled according to the order in which it is identified within the expanded VA procedure framework. For short time lags the VA procedure identifies the smallest ramp scale, so it is referred to as ‘Scale One’, and is designated in the equations with the subscript 1 (Fig. 3a). As the time lag increases, the VA procedure identifies the larger

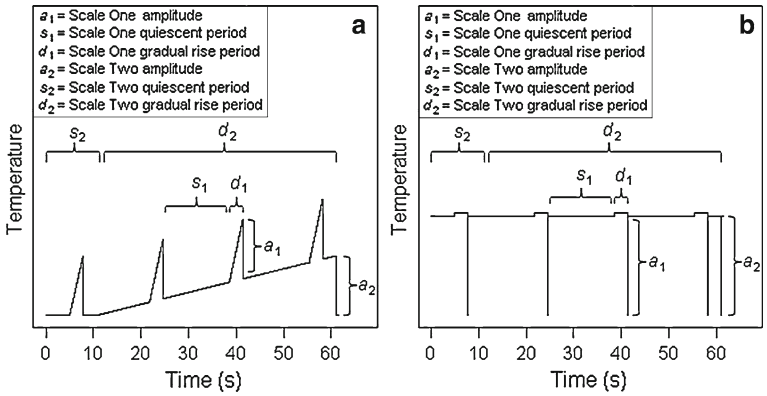

Fig. 3 Traces of **a** a two-scale ramp model and **b** the first-order structure function of a two-scale ramp model

ramp scale, so it is referred to as 'Scale Two', and is designated in the equations with the subscript 2 (Fig. 3a).

To make the derivations of a two-scale ramp model more tractable, six assumptions are made that are in reasonable agreement with turbulent data observations:

(1) Scale One is much shorter than Scale Two, and also shorter than both the quiescent period and the gradual rise period of Scale Two.
(2) Scale One repeats an integer number of times in the quiescent period of Scale Two and an integer number of times in the gradual rise period of Scale Two.
(3) The amplitudes of both ramp scales are equivalent.
(4) The ramps of different scales are offset, so the microfronts of both ramp scales never align. The alignment of the scales causes amplitude modulation. The VA procedure involves the cubed amplitude. Even for the simple case of a one-scale ramp model, amplitude modulation leads to a skew in the magnitude of the VA amplitude solution.
(5) The time lag is much shorter than the quiescent period and gradual rise period of both scales.
(6) The ramp model does not contain a random noise signal. Although real turbulent data contain at least some noise, this assumption simplifies the derivations.

In deriving the structure function, the definite integral is split into two segments (Fig. 3b).

$$\overline{S^n(r)_c} = \frac{1}{(d+s)_2}\left\{\int_0^{s_2}[\Delta T\,(t)]^n\,\mathrm{d}t + \int_{s_2}^{(d+s)_2}[\Delta T\,(t)]^n\,\mathrm{d}t\right\}. \tag{18}$$

The first segment is a function of Scale One only (Fig. 3b), and its value depends on the number of times Scale One repeats for $(0 < t \le s_2)$,

$$\int_0^{s_2}[\Delta T\,(t)]^n\,\mathrm{d}t = \frac{s_2}{(d+s)_1}(-1)^n a_1^n r. \tag{19}$$

In the second segment, both Scale One and Scale Two contribute to the definite integral. Based on the assumptions listed above, it is reasonable to consider: $\left|(-1)^n a_1^n r\right| \gg \left(\frac{a_2 r}{d_2}\right)^n$, allowing the use of the dominant term approximation for Scale One. The contribution of Scale One to

the definite integral is a function of the number of times it repeats for $[s_2 < t \leq (d+s)_2]$. The dominant term approximation also is used to determine the Scale Two contribution to the definite integral, and thus for $[s_2 < t \leq (d+s)_2]$,

$$\int_{s_2}^{(d+s)_2} [\Delta T\,(t)]^n \,\mathrm{d}t = \frac{d_2}{(d+s)_1}\left[(-1)^n a_1^n r\right] + (-1)^n a_2^n r. \tag{20}$$

Substituting Eqs. 19–20 back into Eq. 18 gives the structure function for a two-scale ramp model,

$$\overline{S^n(r)_\mathrm{c}} = \frac{1}{(d+s)_2}\left[\frac{(d+s)_2}{(d+s)_1}(-1)^n a_1^n r + (-1)^n a_2^n r\right]. \tag{21}$$

Thus, the structure function is the weighted average of the dominant terms from both scales.

The next step is to consider the VA procedure for the two-scale ramp model. Substituting the two-scale structure functions into the VA procedure yields the ramp amplitude for both scales. Once the amplitude solution is obtained, the third-order structure-function equation is rearranged, similar to Eq. 10, to determine the VA ramp-period solution,

$$\frac{(d+s)_1}{\left[\frac{(d+s)_1}{(d+s)_2}+1\right]} = -\frac{a^3 r}{\overline{S^3(r)_\mathrm{c}}}. \tag{22}$$

Scale One shortens the VA ramp-period solution relative to the periods of both the Scale One and Scale Two ramps. If a ramp model contains more than one ramp scale, then the VA ramp-period solution is less than the smallest scale ramp period. This occurs because the smallest ramp period is effectively shortened by the presence of the larger ramps, which occasionally interrupt the smaller ramp periods (see Fig. 3b at approximately 60 s). Given that the Scale One ramp period is much shorter than the Scale Two ramp period, the VA ramp period closely approximates the Scale One ramp period.

The VA solutions for two ramp scales can be generalized for other intermittency conditions given that the scales never align and $\left|(-1)^n a_1^n r\right| \gg \left(\frac{a_2 r}{d_2}\right)^n$. If $\left|(-1)^n a_1^n r\right| \gg \left(\frac{a_2 r}{d_2}\right)^n$ is not true, the VA solutions tend to the values of the Scale Two ramp characteristics (not shown).

3.6 The VA Solutions for Scale Two

The ramp characteristics for Scale Two are obtained by solving the VA procedure with a longer structure-function time lag. If Scale One is intermittent, the VA solutions describe Scale Two for $(d_1 \leq r \leq s_1)$. On the other hand, if Scale One is persistent, one arrives at the Scale Two ramp characteristics for $\left[r = \frac{(d+s)_1}{2}\right]$. For a two-scale ramp model with an intermittent Scale One, the definite integral is split into two segments, according to Eq. 18. The time lag is set so that $(d_1 \leq r \leq s_1)$, however, it is assumed that the time lag is still much less than the scale two gradual rise period. In the first segment, only Scale One contributes to the second-order structure function. The integral depends on the number of times Scale One repeats in the first segment, and thus for $(0 < t \leq s_2)$,

$$\int_0^{s_2} [\Delta T\,(t)]^2 \,\mathrm{d}t = \frac{s_2}{(d+s)_1}\left(\frac{2a_1^2 r}{3}\right). \tag{23}$$

In the second segment, the component $\left(\frac{a_2 r}{d_2}\right)^n$ is considered negligible compared to the dominant term of Scale One. The dominant term approximation is invoked for the Scale Two contribution to the definite integral, and for $[s_2 < t \leq (d+s)_2]$,

$$\int_{s_2}^{(d+s)_2} [\Delta T\ (t)]^2\, \mathrm{d}t = \frac{d_2}{(d+s)_1}\left(\frac{2a_1^2 d_1}{3}\right) + a_2^2 r. \tag{24}$$

Therefore, the second-order structure function for a two-scale ramp model with an intermittent Scale One and $d_1 \leq r \leq s_1$ is computed as

$$\overline{S^2(r)_\mathrm{c}} = \frac{2a_1^2 d_1}{3(d+s)_1} + \frac{a_2^2 r}{(d+s)_2}. \tag{25}$$

In the first segment for the odd-ordered structure functions, the contributions by both Scale One and Scale Two are zero (Appendix 2), and in the second segment, the Scale One contribution is zero and $\left(\frac{a_2 r}{d_2}\right)^n$ is assumed negligible. The Scale Two contribution is derived using the dominant term approximation. The odd-ordered structure functions, which do not include Scale One terms, are described as

$$\overline{S^n(r)_\mathrm{c}} = \frac{-a_2^n r}{(d+s)_2}. \tag{26}$$

The second-, third-, and fifth-order structure functions are then passed into the VA procedure. Although the second-order structure function Eq. 25 includes Scale One terms, they interfere negligibly with the VA amplitude solution, and the VA amplitude solution closely approximates the ramp amplitudes of both scales. If the ramp scales have unequal amplitudes, the VA procedure presented here does not close. In the Results section, the efficacy of the VA procedure in resolving the ramp characteristics of both scales is demonstrated despite unequal amplitudes.

The solution of Eq. 26 for the VA ramp period yields the Scale Two ramp period,

$$(d+s)_2 = -\frac{a_2^3 r}{S^3(r)_\mathrm{c}}. \tag{27}$$

If Scale One is persistent, one arrives at the same structure function expressions for $\left[r = \frac{(d+s)_1}{2}\right]$. Thus, for an intermittent Scale One there is a range of time lags for which the VA ramp period resolves the Scale Two characteristics, but in the case of a persistent Scale One there is only one time lag that yields the same results.

3.7 Obtaining the Scale One Gradual Rise Period in a Two-Scale Ramp Model

The gradual rise period of a one-scale ramp model can be obtained following the procedures described in Paw U et al. (2005). If a similar procedure is repeated for a two-scale ramp model based on the same assumptions as previously described, the procedure closely approximates the Scale One gradual rise period.

The previous sections assumed that the time lag was much less than the gradual rise period, so the structure functions are in their linear form. The structure functions are not truncated into their linear form here because the gradual rise period term needs to be retained. Using the dominant term approximation, the third-order structure function of a two-scale ramp model is given by

$$\overline{S^3(r)_c} = -\frac{a^3 r}{(d+s)_1}\left\{\left[1 - \frac{3}{2}\frac{r}{d_1} + \left(\frac{r}{d_1}\right)^2 - \frac{1}{4}\left(\frac{r}{d_1}\right)^3\right] + \frac{(d+s)_1}{(d+s)_2}\left[1 - \frac{3}{2}\frac{r}{d_2} + \left(\frac{r}{d_2}\right)^2 - \frac{1}{4}\left(\frac{r}{d_2}\right)^3\right]\right\}. \quad (28)$$

Following Paw U et al. (2005), the third-order structure function is calculated separately for two time lags, such that one of the time lags is a factor (b) greater than the other. Taking the ratio of both the third-order structure functions (R), cancelling like terms, setting the equation to zero, and simplifying, we obtain,

$$\left(\frac{r}{d_1}\right)^3 - \frac{4\left(R - b^3\right)}{\left(R - b^4\right)}\left(\frac{r}{d_1}\right)^2 + \frac{6\left(R - b^2\right)}{\left(R - b^4\right)}\left(\frac{r}{d_1}\right) - \frac{4(R-b)}{(R-b^4)} + \frac{(d+s)_1}{(d+s)_2}\left\{R\left[1 - \frac{3}{2}\frac{r}{d_2} + \left(\frac{r}{d_2}\right)^2 - \frac{1}{4}\left(\frac{r}{d_2}\right)^3\right] - b\left[1 - \frac{3}{2}\frac{br}{d_2} + \left(\frac{br}{d_2}\right)^2 - \frac{1}{4}\left(\frac{br}{d_2}\right)^3\right]\right\} = 0. \quad (29)$$

Given that Scale One is much shorter than Scale Two, the terms associated with Scale Two's gradual rise period are approximately zero. In which case, Eq. 29 is simplified to,

$$\left(\frac{r}{d_1}\right)^3 - \frac{4\left(R - b^3\right)}{\left(R - b^4\right)}\left(\frac{r}{d_1}\right)^2 + \frac{6\left(R - b^2\right)}{\left(R - b^4\right)}\left(\frac{r}{d_1}\right) - \frac{4(R-b)}{(R-b^4)} = 0, \quad (30)$$

and after solving for the roots of the polynomial and rearranging terms, the Scale One gradual rise period is obtained.

4 Results and Discussion

4.1 Comparison of Derived and Actual Ramp Characteristics

The derived values for the Scale One gradual rise period, the ratio of the Scale One amplitude to the Scale One ramp period, and the ratio of the Scale Two amplitude to the Scale Two ramp period closely agree with the actual values (Table 1). The accurate identification of the ramp characteristics at more than one scale is important to the study of smaller-scale isotropic turbulent processes and larger scale coherent structure transport. The calculated and actual Scale One gradual-rise-period values are generally within a few percent of one another for all the models, and the ratios of the VA solutions for both scales also are in close agreement. Even for the models in which the assumptions are not strictly met, such as M4 – M6, the agreement is close, demonstrating the strength of the expanded VA framework for identifying the ramp characteristics at two scales.

4.2 VA Procedure for the One-Scale Ramp Model

The VA procedure accurately determines the ramp characteristics of M1, the one-scale persistent ramp model, but the accuracy decreases as the time lag increases (Fig. 4a–c). Because M1 makes up Scale Two (i.e., the larger scale) of the other ramp models, it is important to understand the effect of longer time lags on this ramp model. The magnitude of the VA

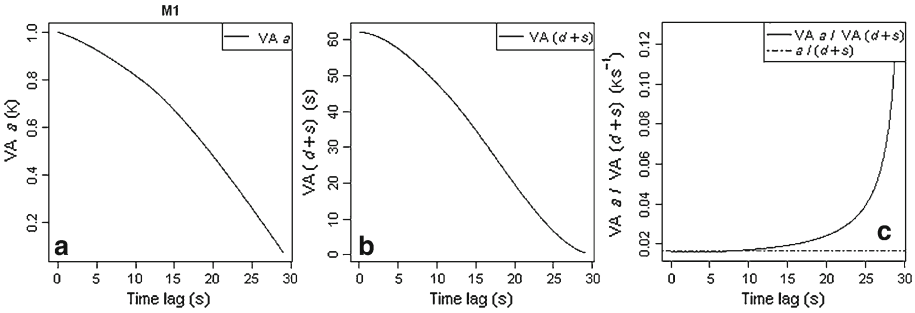

Fig. 4 VA solutions for M1, a one-scale ramp model: **a** VA amplitude for M1, **b** VA ramp period for M1, and **c** VA amplitude divided by the VA ramp period for M1. The *dashed horizontal line* indicates the ramp amplitude divided by the ramp period

amplitude and the VA ramp period decrease with longer time lags because the VA procedure is based on the linear forms of Eqs. 6–8. These equations are less valid as the time lag increases relative to the gradual rise period. Note that the VA solutions approach zero (Fig. 4a–b) as the third-order structure function approaches zero, which occurs at one half of the ramp period (30.5 s in this case). For an intermittent ramp with the same ramp period as M1, the linearization error is more severe over a shorter range of time lags, because the gradual rise period in such a model is shorter, forcing the third-order structure function to zero at a shorter time lag. The ratio of the VA solutions (i.e., the ratio of the VA amplitude to the VA ramp period), which is important in surface renewal calculations, is fairly constant from the shortest time lag near zero to around 10 s (Fig. 4c) despite a marked decrease in the magnitude of the individual terms over the same range. The linearization error affects both VA solutions in a similar fashion, so the ratio of the VA solutions is surprisingly robust for relatively long time lags. In two-scale ramp models the linearization error affects each scale in the same manner as it affects the single scale in a one-scale model.

4.3 Expanded VA Procedure for the Ideal Two-Scale Ramp Models

The six assumptions in the derivations are met in models M2 and M3. The VA solutions over a range of time lags validate the derivations, and demonstrate the efficacy of the expanded VA framework for resolving the ramp characteristics at both scales.

The VA procedure was carried out on M2 for time lags up to one half of the Scale Two ramp period (Fig. 5a–c). Scale Two (i.e., the larger scale) is the same as the ramp in M1, so the general pattern of the VA amplitude and VA ramp period with increasing time lag is similar in Figs. 4a–c and 5a–c. That is, as the time lag increases the VA amplitude slowly decreases due to linearization error, similar to the VA solutions for M1 (Fig. 4a). At the time lags that are much less than the gradual rise period of both scales, the VA amplitude describes the equivalent amplitudes of both scales (Fig. 5a). At the time lag equal to the gradual rise period of Scale One (i.e., the smaller scale), the VA amplitude agrees again with the amplitudes of both scales (Fig. 5a).

The VA ramp period is slightly less than the Scale One ramp period for time lags much less than the gradual rise period of both scales (Table 1; Fig. 5b). This is consistent with Eq. 22, because the left-hand side denominator is inherently >1 for Two Scale ramp models. For the time lag equal to the gradual rise period of Scale One, the VA ramp period identifies the Scale Two ramp period (Fig. 5b). From the time lag equal to the Scale One gradual rise

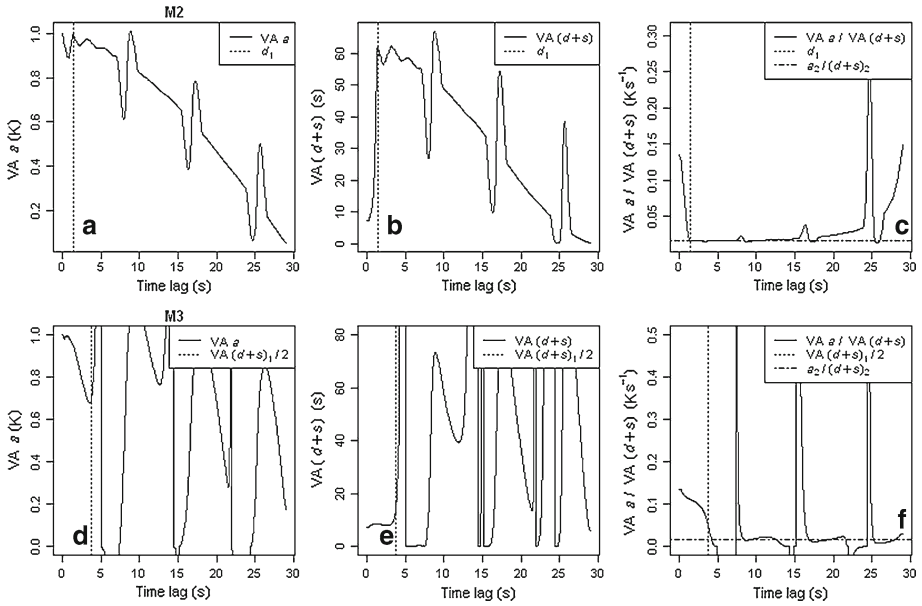

Fig. 5 VA solutions for ramp models M2 and M3: **a** VA amplitude for M2, **b** VA ramp period for M2, **c** VA amplitude divided by the VA ramp period for M2, **d** VA amplitude for M3, **e** VA ramp period for M3, and **f** VA amplitude divided by the VA ramp period for M3. The *dashed vertical line* indicates the calculated Scale One gradual rise period. The *dashed horizontal line* indicates the Scale Two ramp amplitude divided by the Scale Two ramp period

period to the time lag equal to the Scale One quiescent period, Scale One marginally contributes to the structure functions, therefore the VA ramp period corresponds to Scale Two. The linearization error, however, causes a slow decreasing trend in the VA ramp period in this range of time lags, leading to the underestimation of the Scale Two ramp period.

The ratio of the VA amplitude to the VA ramp period shows a precipitous decrease for short time lags (Fig. 5c), and occurs because the VA ramp period rapidly increases (Fig. 5b), while the VA amplitude is fairly constant (Fig. 5a). For the shortest time lags, the ratio of the VA solutions overestimates the ratio of the Scale One ramp characteristics because the VA ramp period underestimates the actual Scale One ramp period. For time lags $\geq$ the Scale One gradual rise period and $\leq$ the Scale One quiescent period, the ratio of the VA amplitude to the VA ramp period closely approximates the ratio of the Scale Two ramp characteristics. It is surprising that the ratio does not change with time lag in this range because the VA amplitude (Fig. 5a) and VA ramp period (Fig. 5b) each individually decrease due to the linearization error. The linearization error, however, affects both terms in a manner that causes the ratio to stay fairly constant, similar to the observation of the VA solutions for M1.

The periodic deviations in the VA amplitude and VA ramp period occur at time lags that are multiples of the Scale One ramp period (Fig. 5a–b). These arise because the Scale One odd-ordered structure functions contribute to the VA solutions near multiples of the Scale One ramp period (Fig. 2b). Without prior knowledge of the ramp scales, one may erroneously interpret the deviations as corresponding to a third scale. It may be possible to further extend the derivation of the VA procedure to ramp scales higher than Scale Two, but such methods are beyond the scope of our study. For now, the identification of more than two ramp scales in turbulence data is only speculative.

The procedure for identifying the Scale Two ramp characteristics is less robust for ramp models with a persistent Scale One, and only one ramp model, M3, has a persistent Scale One. There are two prominent differences between the VA solutions for M3 (Fig. 5d–f) and the VA solutions for the other models. First, the M3 VA solutions (Fig. 5d–f) exhibit extreme fluctuations that extend beyond the limits of the figure axes, and are the result of the Scale One contribution to the odd-ordered structure functions, which for persistent scales are greater than those contributions for intermittent scales. The odd-ordered structure functions cross zero at least twice per completion of the Scale One ramp period (not shown), leading to extreme values in the VA solutions. Second, the VA ramp period does not increase rapidly compared to the VA ramp period of other models (Fig. 5e, f) for the shortest time lags. Instead, the increase occurs at the time lag equal to one half of the Scale One ramp period (see the Theory section). If Scale One is persistent, the identification of the Scale Two characteristics only holds for the time lag equal to one half of the Scale One ramp period, rather than a range of time lags.

To obtain the Scale Two VA solutions from a ramp model with a persistent Scale One, it is necessary to identify one half of the Scale One ramp period. Because the VA procedure slightly underestimates the Scale One ramp period, the calculated value of one half of the Scale One ramp period is also underestimated, and results in a VA amplitude that underestimates the model ramp amplitudes (Fig. 5d). The VA ramp period at this time lag also underestimates the Scale Two ramp period. Because both terms are underestimated, the ratio of the VA amplitude to the VA ramp period agrees fairly well with the actual ratio of these values for Scale Two (Fig. 5f).

The VA solutions for a two-scale ramp model with both scales intermittent and for a two-scale ramp model with a persistent Scale One and an intermittent Scale Two (neither of which are presented herein for the sake of brevity) follow the same patterns as the VA solutions for M2 and M3, respectively. It is therefore the intermittency of Scale One that dictates the stability of the VA solutions for two-scale ramp models.

4.4 The Ramp Spectrum

The ramp spectrum provides qualitative information about the amplitude, frequency, and intermittency of the ramp scales. The frequency with the greatest peak in the ramp spectrum of M2 corresponds to the frequency of the Scale Two (Fig. 6). Because Scale Two (i.e., the larger scale) is persistent, its contribution to the third-order structure function adhered fairly well to the ideal sinusoidal form when plotted against time lag (similar to the third-order structure function in Fig. 2a), and spectral leakage is minimal (Fig. 6). On the other hand, Scale One is intermittent, so its contribution to the third-order structure function was not as sinusoidal as Scale Two (similar to Fig. 2b), and the spectral leakage prominently appears as multiple peaks at the harmonics of the actual ramp frequency (Fig. 6). The frequency corresponding to the Scale One ramp frequency has less amplitude than the amplitude of its second harmonic, and both are less than one half of the model Scale One ramp amplitude. If one does not know a priori the number of ramp scales and the intermittency characteristics of each scale, it is difficult to discern if the ramp spectrum represents a single ramp scale with severe leakage or multiple ramp scales without leakage.

The ramp spectra of the other two-scale models, M3–M6, display similar results (i.e., the intermittency of each scale produces significant leakage and hinders the resolution of the ramp frequencies and amplitudes). The ramp spectrum, however, provides auxiliary

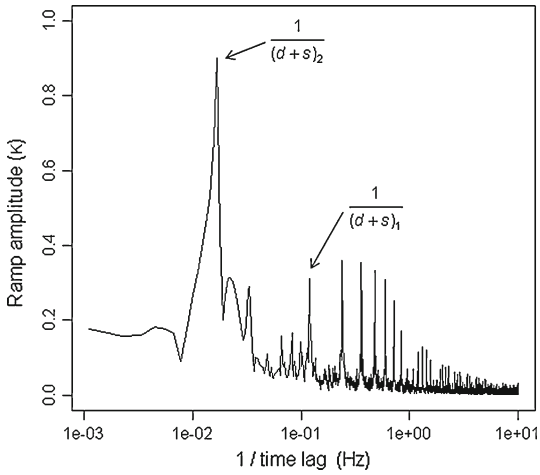

Fig. 6 Ramp spectrum for M2, a two-scale ramp model

information about the ramp scales when used in conjunction with other methods. For example, the VA ramp period solutions for Scale One and Scale Two can be checked against the ramp spectrum. In future studies, it may prove useful to use quantitative methods for processing the ramp spectrum.

4.5 Expanded VA Procedure for the Non-ideal Two-Scale Ramp Models

Although ramp models M4–M6 do not strictly meet the assumptions in the derivations, the VA solutions agree well with the solutions predicted in the Theory section. The ramp amplitudes of the two scales are unequal in M4 (Table 1), so the VA amplitudes at the shortest time lag and at the time lag equal to the Scale One gradual rise period are weighted according to the Scale One and Scale Two ramp amplitudes, respectively (Fig. 7a). The Scale One VA ramp period is overestimated (Fig. 7b), leading to an underestimation of the ratio of the Scale One VA solutions (Fig. 7c), while the Scale One gradual rise period is marginally overestimated using Eq. 30 (Table 1; Fig. 7a). The VA ramp period at the time lag equal to the derived Scale One gradual rise period correctly identifies the Scale Two ramp period (Fig. 7b). The ratio of the ramp characteristics at the time lags between the gradual rise period and quiescent period of Scale One agree well with the ratio of the Scale Two ramp characteristics (Fig. 7c). The periodic spikes arising from the Scale One periodicity are less pronounced in comparison to the VA solutions for M2 (Fig. 5a–c). This occurs because the Scale One ramp amplitude in M4 is relatively small, so it affects the structure functions to a lesser degree than in other models.

In the fifth ramp model, M5, the assumption that the Scale One ramp period is much less than the Scale Two ramp period is violated (Table 1) and reflects what is sometimes observed in actual turbulent data. The VA amplitude correctly identifies the Scale One ramp amplitude (Fig. 7d), and is expected given that none of the assumptions about the ramp amplitude or the alignment of ramp scales is broken. The VA ramp period underestimates the Scale One ramp period, because the denominator in Eq. 22 is >1; the ratio of the VA amplitude to the VA ramp period for Scale One is, therefore, overestimated. At the time lag equal to the derived

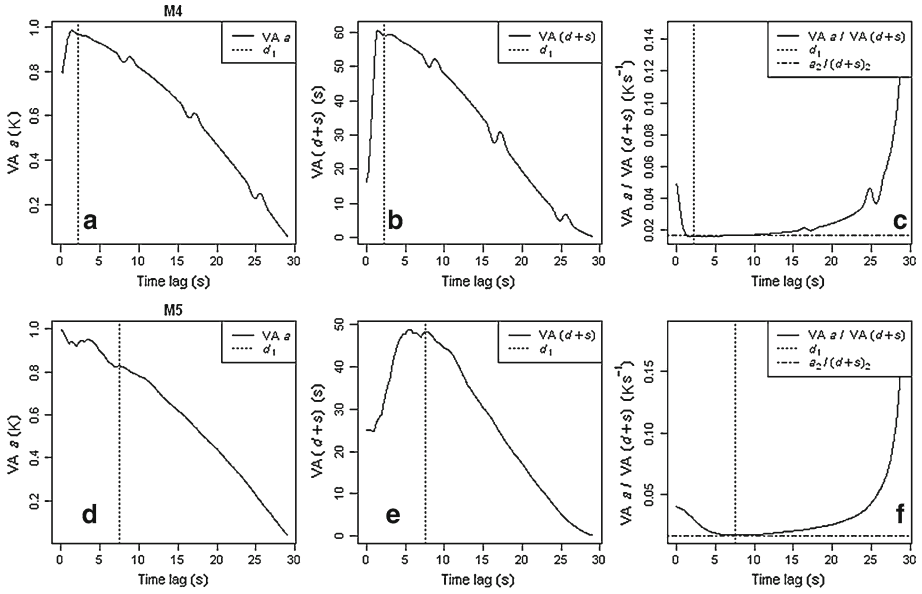

Fig. 7 VA solutions for ramp models M4 and M5: **a** VA amplitude for M4, **b** VA ramp period for M4, **c** VA amplitude divided by the VA ramp period for M4, **d** VA amplitude for M5, **e** VA ramp period for M5, and **f** VA amplitude divided by the VA ramp period for M5. The *dashed vertical line* indicates the calculated Scale One gradual rise period. The *horizontal line* indicated the Scale Two ramp amplitude divided by the Scale Two ramp period

Scale One gradual rise period, the VA amplitude underestimates the Scale Two ramp amplitude; this is the result of the linearization error, which is confirmed by comparing the VA amplitudes of M1 (Fig. 4a) and M5 (Fig. 7d). The Scale One gradual rise period is overestimated, which is consistent with Eq. 28, because the terms associated with Scale Two's gradual rise period are no longer approximately zero. At this time lag, the Scale Two VA ramp period underestimates the actual Scale Two ramp period due to the underestimation of the Scale Two VA amplitude. With both the Scale Two VA amplitude and VA ramp period attenuated by the linearization error, the ratio of the two terms agrees well with the ratio of the actual Scale Two ramp characteristics. Departures from the two-scale ramp model assumptions affect the third-order structure function, the VA amplitude solution, and the VA ramp period solution in concert, making the ratio of the VA amplitude solution to the VA ramp period solution for both scales surprisingly robust.

Alternative small-scale waveforms (such as might be expected from small-scale random turbulence) cause similar phenomena as those seen in the VA solutions for the previous two-scale models (M2–M5), as long as there is a sudden fall in the terminus of the smaller waveform. For example, an intermittent spike resembling the VA ramp model, except the gradual rise period is initiated with a sudden fall, is superimposed on M1 to create M6 (Fig. 8a). Although the shape of this small-scale waveform is similar to a ramp, it may be interpreted as representing isotropic noise because the decrease in temperature is equal to the increase in temperature (i.e., it is symmetric). The ratio of the VA amplitude to the VA ramp period decreases precipitously for short time lags (Fig. 8b), arriving at the ratio of the Scale Two amplitude to the Scale Two ramp period at the time lag close to the Scale One gradual rise period.

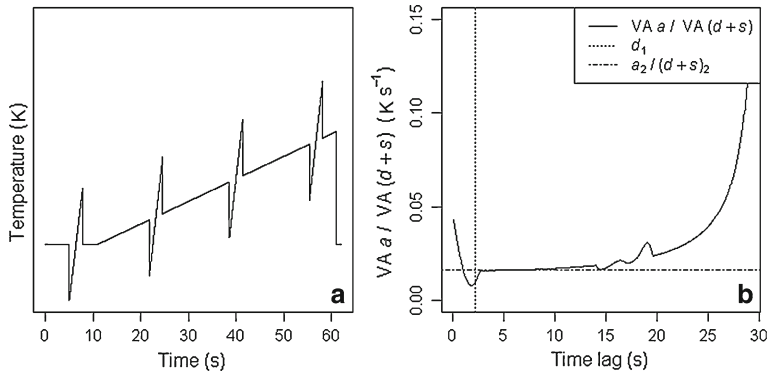

Fig. 8 **a** Trace of M6, a two-scale ramp model with an alternative small-scale waveform superimposed on it, and **b** VA amplitude divided by the VA ramp period for M6. The *dashed vertical line* indicates the calculated Scale One gradual rise period. The *dashed horizontal line* indicates the Scale Two ramp amplitude divided by the Scale Two ramp period

5 Conclusions

The structure functions of the VA ramp model were expanded to include the equations for the complete range of time lags. Owing to the periodicity of the ramps in the time series, the structure functions also exhibited a periodicity, which happens to loosely resemble a sine wave for odd-ordered structure functions. Qualitative information about the ramp scales can be obtained from the DFT of the third-order structure function and the ramp spectrum.

The structure functions for a two-scale ramp model were derived, with Scale One representing smaller size non-flux-bearing turbulence, and the larger Scale Two representing the main flux-bearing eddies. The VA solutions depend on the time lag for both one-scale and two-scale ramp models. In a two-scale model the linearization error affects the VA solutions of each scale in the same manner as it affects the VA solutions in a one-scale model. The ramp characteristics of Scale One are obtained from the classical VA procedure based on very short time lags, while the ramp characteristics of Scale Two are obtained by increasing the time lag parameter. Compared to the VA solutions for ramp models with a persistent Scale One, the VA solutions for ramp models with an intermittent Scale One provide a more reliable estimate of the Scale Two ramp characteristics over a broader range of time lags. The derivations of the structure functions and expanded VA procedure provide robust predictions of the VA solutions at both scales. Alternative smaller scale waveforms that terminate with a sudden decrease produce similar results in the VA solutions as the two-scale ramp models. The theory presented here is used in Part II of this study (Shapland et al. 2012) to develop a scheme for the objective identification of the ramp characteristics at Scale One and Scale Two.

Acknowledgments Partial support for this research was provided by J. Lohr Vineyards & Wines, the National Grape and Wine Institute, a NIFA Specialty Crops Research Initiative grant, USDA-ARS CRIS funding (Research Project #5306-21220-004-00), and the Lindbergh Foundation.

Appendix 1: Complete Structure Functions for Persistent Ramps

The first set of structure functions is for persistent ramps (Fig. 1a). For time lag equal to zero, the coherent structure functions are identically zero. Next, the originally derived Van Atta

(1977) equations are considered. For the time lag less than the quiescent period less than the warming period ($r < s < d$),

$$\overline{S^n(r)_c} = \frac{1}{(d+s)} \left\{ \int_{(s-r)}^{s} \left[\frac{a}{d}(t-s+r)\right]^n \mathrm{d}t + \int_{s}^{(d+s-r)} \left[\frac{ar}{d}\right]^n \mathrm{d}t + \int_{(d+s-r)}^{(d+s)} \left[\frac{a}{d}(s-t)\right]^n \mathrm{d}t \right\}, \tag{31}$$

where integration for each power and simplification yields Eqs. 6–8.

For the quiescent period less than the time lag less than the warming period ($s < r < d$),

$$\overline{S^n(r)_c} = \frac{1}{(d+s)} \left\{ \int_{0}^{s} \left[\frac{a}{d}(t-s+r)\right]^n \mathrm{d}t + \int_{s}^{(d+s-r)} \left[\frac{ar}{d}\right]^n \mathrm{d}t + \int_{(d+s-r)}^{(d+2s-r)} \left[\frac{a}{d}(s-t)\right]^n \mathrm{d}t + \int_{(d+2s-r)}^{(d+s)} \left[-\frac{a}{d}(d+s-r)\right]^n \mathrm{d}t \right\}, \tag{32}$$

where integration yields

$$\overline{S^2(r)_c} = \frac{a^2}{3d^2(d+s)} \left[r^3 - (r-s)^3 + (r-d)^3 + (d+s-r)^3 + 3r^2(d-r) - 3(d+s-r)^2(s-r)\right], \tag{33}$$

$$\overline{S^3(r)_c} = \frac{a^3}{4d^3(d+s)} \left[r^4 - (r-s)^4 + (r-d)^4 - (d+s-r)^4 + 4r^3(d-r) + 4(d+s-r)^3(s-r)\right], \tag{34}$$

$$\overline{S^5(r)_c} = \frac{a^5}{6d^5(d+s)} \left[r^6 - (r-s)^6 + (r-d)^6 - (d+s-r)^6 + 6r^5(d-r) + 6(d+s-r)^5(s-r)\right]. \tag{35}$$

For the quiescent period less than the warming period less than the time lag ($s < d < r$),

$$\overline{S^n(r)_c} = \frac{1}{(d+s)} \left(\int_{0}^{(d+s-r)} \left[\frac{a}{d}(t-s+r)\right]^n \mathrm{d}t + \int_{s}^{(d+2s-r)} \left[\frac{a}{d}(s-t)\right]^n \mathrm{d}t + \int_{(d+2s-r)}^{(d+s)} \left[-\frac{a}{d}(d+s-r)\right]^n \mathrm{d}t \right), \tag{36}$$

where integration yields

$$\overline{S^2(r)_c} = \frac{a^2}{3d^2(d+s)}\left[d^3 - (r-s)^3 + (d+s-r)^3 - 3\,(d+s-r)^2\,(s-r)\right], \quad (37)$$

$$\overline{S^3(r)_c} = \frac{a^3}{4d^3(d+s)}\left[d^4 - (r-s)^4 - (d+s-r)^4 + 4\,(d+s-r)^3\,(s-r)\right], \quad (38)$$

$$\overline{S^5(r)_c} = \frac{a^5}{6d^5(d+s)}\left[d^6 - (r-s)^6 - (d+s-r)^6 + 6\,(d+s-r)^5\,(s-r)\right]. \quad (39)$$

For time lags equal to multiples of the ramp period [$r = k(d+s)$, where k is an integer], the structure functions are equal to zero.

Appendix 2: Complete Structure Functions for Intermittent Ramps

The second set of structure functions apply to intermittent ramps (Fig. 1b). For a time lag equal to zero, the structure functions are equal to zero.

For time lags less than the gradual rise period, and in turn less than the quiescent period ($r < d < s$), the structure functions are equivalent to the structure functions for the persistent ramp model (Eqs. 6–8). Because the linear forms of the structure functions for short time lags regardless of intermittency conditions are equivalent, the VA procedure is applicable to both persistent and intermittent ramp models.

For the gradual rise period less than the time lag less than the quiescent period ($d < r < s$), the structure functions are

$$\overline{S^n(r)_c} = \frac{1}{(d+s)}\left\{\int_{s-r}^{(d+s-r)}\left[\frac{a}{d}\,(t-s+r)\right]^n \mathrm{d}t + \int_{s}^{(d+s)}\left[\frac{a}{d}\,(s-t)\right]^n \mathrm{d}t\right\}, \quad (40)$$

where integration yields

$$\overline{S^2(r)_c} = \frac{2a^2d}{3(d+s)} \quad (41)$$

for the second-order structure function. The odd-ordered structure functions are zero.

For the gradual rise period less than the quiescent period less than the time lag ($d < s < r$), the structure functions are equivalent to the structure functions for persistent ramp models (see Eqs. 37–39). For time lags equal to multiples of the ramp period [$r = k(d+s)$, where k is an integer], the structure functions are zero.

References

Antonia RA, Rajagopalan A, Chambers AJ (1983) Conditional sampling of turbulence in the atmospheric surface layer. J Clim Appl Meteorol 22:69–78

Blackwelder RF, Kaplan RE (1976) On the wall structure of the turbulent boundary layer. J Fluid Mech 76:89–112

Bloomfield P (2000) Fourier analysis of time series. Wiley, New York, 288 pp

Chen W, Novak MD, Black TA (1997a) Coherent eddies and temperature structure functions for three contrasting surfaces. Part I: Ramp model with finite microfront time. Boundary-Layer Meteorol 84:99–123

Chen W, Novak MD, Black TA (1997b) Coherent eddies and temperature structure functions for three contrasting surfaces. Part II: Renewal model for sensible heat flux. Boundary-Layer Meteorol 84:125–147

Collineau S, Brunet Y (1993a) Detection of turbulent coherent motions in a forest canopy. Part I: Wavelet analysis. Boundary-Layer Meteorol 65:357–379
Collineau S, Brunet Y (1993b) Detection of turbulent coherent motions in a forest canopy. Part II: Time-scales and conditional averages. Boundary-Layer Meteorol 66:49–73
Gao W, Shaw RH, Paw U KT (1989) Observations of organized structure in turbulent flow within and above a forest canopy. Boundary-Layer Meteorol 47:349–377
Lenschow DH (1986) Probing the atmospheric boundary layer. American Meteorological Society, Boston, 269 pp
Monin AS, Yaglom AM (1975) Statistical fluid mechanics II. MIT Press, Cambridge, 874 pp
Paw U KT (2001) Coherent structures and surface renewal. In: Rossi F, Duce P, Spano D (eds) Advanced short course on agricultural forest and micro meteorology. Consiglio Nazionale delle Richerche, Sassari, 304 pp
Paw U KT, Brunet Y, Collineau S, Shaw RH, Maitani T, Qui J, Hipps L (1992) On coherent structures in turbulence above and within agricultural plant canopies. Agric For Meteorol 61:55–68
Paw U KT, Qiu J, Su HB, Watanabe T, Brunet Y (1995) Surface renewal analysis: a new method to obtain scalar fluxes without velocity data. Agric For Meteorol 74:119–137
Paw U KT, Snyder RL, Spano D, Su HB (2005) Surface renewal estimates of scalar exchange. In: Hatfield JL (ed) Micrometeorology of agricultural systems. Agronomy Society of America, Madison, 584 pp
R Development Core Team (2012) R: A language and environment for statistical computing. R Foundation for Statistical Computing, Vienna. ISBN3-900051-07-0
Shapland TM, McElrone AI, Snyder RL, Paw U KT (2012) Structure function analysis of two-scale scalar ramps. Part II: Ramp characteristics and surface renewal flux estimation. Boundary-Layer Meteorol 145 (this issue)
Snyder RL, Spano D, Paw U KT (1996) Surface renewal analysis of sensible and latent heat flux density. Boundary-Layer Meteorol 77:249–266
Snyder RL, Paw U KT, Spano D, Duce P (1997) Surface renewal estimates of evapotranspiration. Acta Hortic 449:49–55
Spano D, Snyder RL, Duce P, Paw U KT (1997) Surface renewal analysis for sensible heat flux density using structure functions. Agric For Meteorol 86:259–271
Spano D, Snyder RL, Duce P, Paw U KT (2000) Estimating sensible and latent heat flux densities from grapevine canopies using surface renewal. Agric For Meteorol 104:171–183
Stull RB (1988) An introduction to boundary layer meteorology. Kluwer Academic Publishers, Dordrecht, 666 pp
Thomas C, Mayer JC, Meixner FX, Foken T (2006) Analysis of low-frequency turbulence over tall vegetation using a Doppler sodar. Boundary-Layer Meteorol 119:563–587
Van Atta CW (1977) Effect of coherent structures on structure functions of temperature in the atmospheric boundary layer. Arch Mech 29:161–171
Wyngaard JC (1973) On surface-layer turbulence. In: Haugen DA (ed) Workshop on micrometeorology. American Meteorological Society, Boston pp 101–149
Wyngaard JC (2010) Turbulence in the atmosphere. Cambridge University Press, Cambridge, 393 pp
Wyngaard JC, Lemone MA (1980) Behavior of the refractive index structure parameter in the entraining boundary layer. J Atmos Sci 37:1573–1585
Wyngaard JC, Cote OR, Izumi Y (1971) Local free convection, similarity, and the budgets of shear stress and heatflux. J Atmos Sci 28:1171–1182